3D Palmprint Identification Using Block-Wise Features and Collaborative Representation

Lin Zhang, *Member, IEEE*, Ying Shen, *Member, IEEE*, Hongyu Li, and Jianwei Lu

Abstract—Developing 3D palmprint recognition systems has recently begun to draw attention of researchers. Compared with its 2D counterpart, 3D palmprint has several unique merits. However, most of the existing 3D palmprint matching methods are designed for one-to-one verification and they are not efficient to cope with the one-to-many identification case. In this paper, we fill this gap by proposing a collaborative representation (CR) based framework with l_1-norm or l_2-norm regularizations for 3D palmprint identification. The effects of different regularization terms have been evaluated in experiments. To use the CR-based classification framework, one key issue is how to extract feature vectors. To this end, we propose a block-wise statistics based feature extraction scheme. We divide a 3D palmprint ROI into uniform blocks and extract a histogram of surface types from each block; histograms from all blocks are then concatenated to form a feature vector. Such feature vectors are highly discriminative and are robust to mere misalignment. Experiments demonstrate that the proposed CR-based framework with an l_2-norm regularization term can achieve much better recognition accuracy than the other methods. More importantly, its computational complexity is extremely low, making it quite suitable for the large-scale identification application. Source codes are available at http://sse.tongji.edu.cn/linzhang/cr3dpalm/cr3dpalm.htm.

Index Terms—3D palmprint, sparse representation, l_1-minimization, collaborative representation, surface type

1 Introduction

Bolstered by the requirements of numerous applications, such as access control, aviation security, or e-banking, recognizing the identity of a person with high confidence has become a topic of intense study. To solve such a problem, biometrics based approaches are drawing more and more attention. As an important member of the biometrics family, the palmprint has been corroborated to have the merits of high distinctiveness, robustness, and high user-friendliness, etc. Palmprint refers to the skin patterns on the inner palm surface, comprising mainly two kinds of features: the palmar friction ridges (the ridge and valley structures like the fingerprint) and the palmar flexion creases (discontinuities in the epidermal ridge patterns) [1]. Both of these two features are deemed to be immutable, permanent, and unique to each individual [2]. Actually, the use of palmprints for personal authentication can trace back to Chinese deeds of sale in the 16th century [3]. In this paper, our aim is to develop an efficient and effective personal identification approach based on 3D palmprints.

1.1 Related Works

In the past decade, researchers have made tremendous efforts in developing automatic palmprint-based personal authentication schemes. Several representative ones are briefly reviewed here. The majority of the existing palmprint recognition systems were developed for civilian applications, mainly access control. Typically, these systems utilize low resolution images, about 100 ppi. At such a low resolution, ridges cannot be observed and matching is mainly based on principal lines and creases. In Zhang et al.'s salient work [4], they created an online palmprint recognition system, which uses pegs to fix hand position and detects finger gaps to facilitate alignment. By using the developed device, they established the PolyU 2D palmprint data set [5], which has been widely used in the literature. Later, different kinds of methods for palmprint matching have been proposed and validated on the PolyU data set, including line-based ones [6], subspace-based ones [7], [8], statistics-based ones [9], and coding-based ones [10], [11], [12], [13]. In [14], Michael et al. developed a contactless palmprint recognition system and for matching they applied the LBP (local binary pattern) [15] texture descriptor to image's directional gradient responses.

Quite recently, several research groups have begun developing automatic matching methods for latent palmprints, which are used mainly for forensic applications. In forensic applications, 500 ppi is the standard image resolution [16]. Ridge structures can be clearly observed on these images and thus matching schemes designed for these high resolution palmprint images are usually based on ridges. Representative works in this field can be found in [1], [17], [18].

Actually, the aforementioned research on palmprint recognition mainly concentrates on 2D palmprint images. Though they may have already been successfully used in many applications, 2D palmprint based recognition systems have several inherent drawbacks. At first, the quality of 2D images suffers from changes in imaging factors such as illumination. Second, although the area of the palm is relatively large, too much contamination on the palm can still substantially affect the recognition result. More seriously, 2D palmprint based systems are vulnerable to various kinds of attacks since 2D palmprint images can be easily copied and counterfeited. In order to overcome these intrinsic problems of 2D palmprints, 3D palmprint based personal authentication techniques have recently been developed [19], [20], [21], [22], [23], [24], [25], [26], [27].

In [19], [20], Li et al. invented a 3D palmprint acquisition device by using structured-light technology, with which the 3D range data and the 2D texture data could be simultaneously acquired from a palm. The outlook of such a device is shown in Fig. 1. By using the developed device, Li et al. have established a large-scale 3D palmprint data set [21]. For matching 3D palmprints, different schemes have been proposed. In [20], mean curvature images (MCI), Gaussian curvature images (GCI), and surface type (ST) maps were computed and for matching the authors defined two metrics, similar as Hamming distance [28]. In [22], Li et al. extracted three levels of 2D and 3D palmprint features, including shape features, principal line features, and texture features. To account for small alignment errors, they performed alignment refinement to the feature maps by using ICP (iterative closest point) [29]. The apparent drawback of this method lies in its high computational complexity. In their another work [23], Li et al. computed the MCI from the original range data at first and then extracted both line and orientation features from MCI. After that, two types of features were fused at either score level or feature level for matching. In [24], Zhang et al. proposed a multi-level framework for personal authentication by combining 2D and 3D palmprint features. For comparing two 3D palmprints, they at first extracted surface curvature maps and then used the normalized local correlation for matching. In [25], Yang et al. utilized the shape index representation to describe the geometry of local regions in a 3D palmprint and they extracted LBP [15] and Gabor wavelet features from the shape index image. Then, those two features were finally fused at score level. In [26], for feature extraction, Liu and Li applied the OLOF (orthogonal line ordinal feature) operator [11]

- *L. Zhang is with the School of Software Engineering, Tongji University, Shanghai 201804, China and also with the Jiangsu Key Laboratory of Image and Video Understanding for Social Safety, Nanjing, University of Science and Technology, Nanjing 210094, China. E-mail: cslinzhang@tongji.edu.cn.*
- *Y. Shen and H. Li are with the School of Software Engineering, Tongji University, Shanghai 201804, China. E-mail: {yingshen, hyli}@tongji.edu.cn.*
- *J. Lu is with the Advanced Institute of Translational Medicine and the School of Software Engineering, Tongji University, Shanghai 201804, China. E-mail: jwlu33@gmail.com.*

Manuscript received 29 June 2014; revised 26 Sept. 2014; accepted 13 Nov. 2014. Date of publication 23 Nov. 2014; date of current version 6 July 2015.
Recommended for acceptance by D. Maltoni.
For information on obtaining reprints of this article, please send e-mail to: reprints@ieee.org, and reference the Digital Object Identifier below.
Digital Object Identifier no. 10.1109/TPAMI.2014.2372764

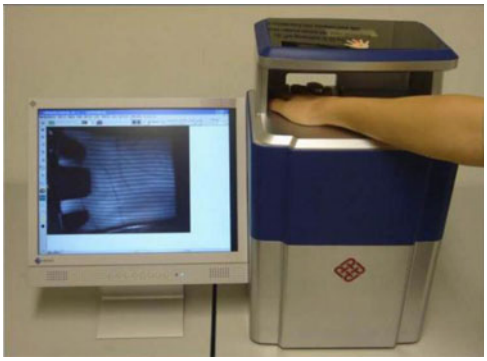

Fig. 1. 3D palmprint acquisition device developed in [19].

on MCI derived from a 3D palmprint. To account for small misalignment between two palmprint samples, they tried to use a cross correlation based method to register two feature maps. In [27], Cui proposed a 2D plus 3D palmprint recognition system by using the two-phase test sample representation (TPTSR) framework [30].

It needs to be noted that in addition to 3D palmprint, there are also some other 3D biometric technologies developed in recent years, such as 3D face [31], [32] and 3D ear [33], [34]. Compared with them, 3D palmprint has some inherent advantages. For example, compared with 3D face, 3D palmprint is not affected by the challenges associated with various facial expressions; compared with 3D ear, 3D palmprint is much easier to be collectedly and is more user-friendly.

1.2 Our Motivations and Contributions

From the abovementioned introduction, it can be seen that all the state-of-the-art 3D palmprint matching methods share a common paradigm: when matching two 3D palmprints, two corresponding feature maps will be extracted from the range data and their matching score will be computed by using a pre-defined metric; for dealing with small misalignments, multi-translation-based matching [20], [23] or explicit registration techniques [22], [26] are used. These methods are quite suitable for the one-to-one verification application. When these methods are used for the one-to-many identification application, to figure out the identity of a given test sample, it would be necessary to match the test sample to all the samples in the gallery set one by one. Such a brute-force searching strategy is obviously not quite computationally efficient, especially when the size of the gallery set is extremely large. Consequently, in this paper, our aim is to develop an efficient 3D palmprint classification strategy, which can be deployed in large-scale identification applications.

Actually, the task of identification is essentially to find out a single class containing samples most similar to the input test sample out of the entire gallery set. To solve such a one-to-many identification problem, recent studies have found that the sparse representation based classification (SRC) is an effective and efficient tool [34], [35], [36], [37], [38], [39]. For example, in [35], Wright et al. reported an impressive work for face recognition by using SRC. With their method, a query face image is first sparsely coded over the gallery images, and then the classification is performed by checking which class yields the least coding error. Sparse representation codes a signal $\boldsymbol{y}$ over a dictionary $\mathbf{A}$ such that $\boldsymbol{y} \approx \mathbf{A}\boldsymbol{\alpha}$ and $\boldsymbol{\alpha}$ is a sparse coefficient vector. The sparsity of $\boldsymbol{\alpha}$ can be measured by l_0-norm, which counts the number of non-zeros in $\boldsymbol{\alpha}$. Since the l_0-minimization is NP-hard, the l_1-minimization, as the closest convex function to the l_0-minimization [40], is widely employed in sparse coding. However, some recent studies have started to question the necessity of the l_1-norm sparsity regularization in the SRC model [41], [42]. In [42], Zhang et al. analyzed deeply the working mechanism of SRC and claimed that it is the collaborative representation (CR, i.e., using the gallery samples from all classes to represent the query sample $\boldsymbol{y}$) but not the l_1-norm sparsity that makes SRC powerful for face recognition. And accordingly, they proposed to replace the l_1-norm sparsity regularization term in SRC framework with an l_2-norm regularization term and such a classification scheme is called CRC_RLS (collaborative representation based classification with regularized least square). Zhang et al.'s experimental results indicate that CRC_RLS could achieve comparable recognition accuracy as SRC; however, CRC_RLS performs greatly faster than SRC [42]. The reason is that for CRC_RLS, there exists a simple closed-form solution while by contrast solving SRC will involve a costly iterative optimization.

On seeing that CRC_RLS or SRC are quite promising classification schemes, in this paper, we propose to adapt them for 3D palmprint identification. To our knowledge, this is the first work attempting to make use of collaborative representation based classification schemes for 3D palmprint identification and their validity has been corroborated in our experiments. Our experimental results indicate that no matter l_1-norm or l_2-norm regularization is used, the proposed CR-based 3D palmprint identification approaches perform much better than the other state-of-the-art methods. Particularly, the l_2-norm regularization based CR method (i.e., CRC_RLS) could achieve quite similar recognition accuracy as the l_1-norm regularization based CR method (i.e., SRC) while the former performs much faster.

To use CR-based classification schemes (no matter l_1-norm or l_2-norm regularization is used), how to extract feature vectors to represent 3D palmprints is a critical issue. Since there exists mere misalignment between two palmprint ROIs (region of interest), the extracted feature vectors should be robust to small misalignment while maintaining a high discriminative capability. To meet these requirements, we propose a novel block-wise statistics based feature extraction scheme. Specifically, we at first divide a 3D palmprint ROI into uniform blocks and extract a histogram of surface types [43] from each block; histograms from all the blocks are then concatenated to form a feature vector. Such feature vectors are highly discriminative and are robust to mere misalignment between samples.

The effectiveness and the efficiency of the proposed 3D palmprint recognition schemes have been corroborated by extensive experiments conducted on PolyU 3D palmprint data set [21]. To make the results reproducible, Matlab source codes and associated evaluation results have been made publicly available online at http://sse.tongji.edu.cn/linzhang/cr3dpalm/cr3dpalm.htm.

The remainder of this paper is organized as follows. Section 2 introduces the block-wise statistics based features used in our method. Section 3 presents the structure of our CR-based 3D palmprint identification scheme. Section 4 reports the experimental results. Finally, Section 5 concludes the paper.

2 Block-Wise Statistics Based Features

In this section, the feature extraction method used in our system will be introduced in details, which is a critical component in our 3D palmprint identification scheme. It needs to be noted that the feature extraction is applied to ROIs of 3D palmprints, which are provided by PolyU 3D palmprint data set [21].

For face recognition, CR-based classification schemes (SRC [35] or CRC_RLS [42]) typically use vectorized raw image pixels as feature vectors and pleasing results could be obtained. However, actually these methods require that the test image and the training set must be well aligned. As reported in [36], if the test image has even a small amount of registration error against training images (which is also true for the 3D palmprint classification problem), the representation coefficients will no longer be informative. To deal with this problem, several studies have been conducted recently. In [36], Wagner et al. solve this challenging issue by a series of linear

TABLE 1
ST Labels Defined by Signs of Surface Curvatures [43]

	$K>0$	$K=0$	$K<0$
$H<0$	Peak (ST = 1)	Ridge (ST = 2)	Saddle Ridge (ST = 3)
$H=0$	None (ST = 4)	Flat (ST = 5)	Minimal Surface (ST = 6)
$H>0$	Pit (ST = 7)	Valley (ST = 8)	Saddle Valley (ST = 9)

programs that iteratively minimize the sparsity of the registration error. In [37], Peng et al. formulate the batch image alignment as searching for a set of transformations that can minimize the rank of the transformed images, which are viewed as columns of a matrix. If Wagner et al.'s method [36] or Peng et al.'s method [37] is adopted, the misalignment between the test image and images of each training class needs to be rectified explicitly. Obviously, this is quite time consuming and thus is not suitable for large-scale identification applications.

As pointed out by Li et al., though the ROI extraction procedure can align the palmprints to some extent, there are still mere misalignments between ROIs [22]. Since explicitly registering the test palmprint sample to the training samples is extremely time-consuming, we expect to find a new feature extraction scheme which is robust to mere misalignments while the extracted feature vectors are also highly discriminative. To meet these requirements, we propose a novel 3D feature extraction scheme based on block-wise statistics, whose details will be presented in the following.

A 3D palmprint can be considered as a surface with various convex and concave structures. We can classify the points on the palmprint into different types based on their different geometric characteristics. Such a kind of 3D feature is called as surface type [43], which has been proved to be highly discriminative. Assume that a 3D palmprint ROI is represented by $S(x, y, f(x, y))$. Mean curvature H and Gaussian curvature K can be computed as [44],

$$H = \frac{\left(1+f_x^2\right)f_{yy} + \left(1+f_y^2\right)f_{xx} - 2f_x f_y f_{xy}}{2\left(1+f_x^2+f_y^2\right)^{3/2}} \tag{1}$$

$$K = \frac{f_{xx}f_{yy} - f_{xy}^2}{\left(1+f_x^2+f_y^2\right)^2}, \tag{2}$$

where $f_x(f_y), f_{xx}(f_{yy}, f_{xy})$ are the first order and second order partial derivatives, respectively. There are eight fundamental viewpoint independent surface types that can be characterized using only the sign of the mean curvature (H) and Gaussian curvature (K) [43]. For completeness, we list their definitions in Table 1. In total, nine STs can be defined, including eight fundamental STs and one special case for $H = 0$ and $K > 0$.

With the abovementioned procedures, each point in the 3D palmprint ROI can be classified into one of the nine STs. Thus, for each 3D palmprint ROI, we could obtain a ST map, each field of which is an integer from 1 to 9. Examples of ST maps are shown in Fig. 2. In Fig. 2, the first row displays three 3D palmprint ROIs, shown in image format while the second row displays their corresponding ST maps. Fig. 2a and 2b are captured from the same palm but in different sessions while Fig. 2b and 2c are captured from different palms.

As a 3D feature, surface type maps are highly discriminative but they are sensitive to small amount of registration errors between the test image and training images. On the other hand, global statistics based features, such as histograms and moment invariants [45], are robust to misalignments but they are not quite discriminative. In order to integrate the merits of these two kinds of feature extraction schemes, we propose to use block-wise ST statistics based features.

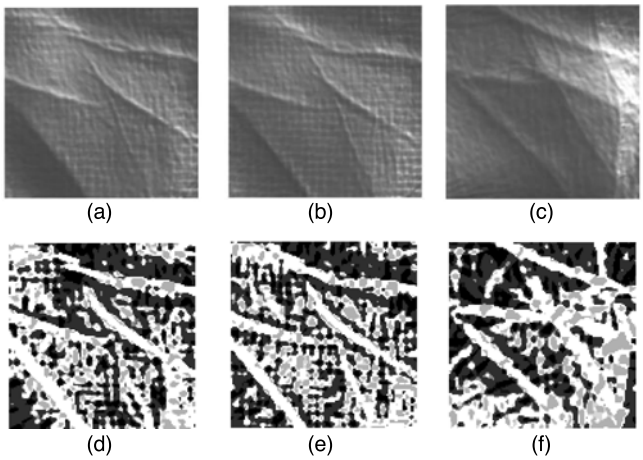

Fig. 2. The first row displays three 3D palmprint ROIs, shown in image format while the second row displays their corresponding ST maps. (a) and (b) are captured from the same palm but in different sessions. (b) and (c) are from different palms.

Suppose that for a 3D palmprint ROI, we have computed from it a ST map M. Then, we uniformly divide M into a set of $p \times p$ blocks. For each block i, we compute from it a histogram of surface types, denoted by $\boldsymbol{h}_i$. Obviously, the dimension of $\boldsymbol{h}_i$ is nine since there are totally nine possible surface types (see Table 1). Finally, all $\boldsymbol{h}_i$s are concatenated together as a large histogram $\boldsymbol{h}$, which is considered to be the feature vector. Experimental results have corroborated the efficacy of such a feature extraction scheme (see Section 4).

3 CR-Based 3D Palmprint Identification

By using the proposed feature extraction scheme as presented in Section 2, given a 3D palmprint gallery set, we can compute a feature vector for each sample in the gallery set and then we can define a dictionary matrix $\mathbf{A}$ for the entire gallery set as the concatenation of all the extracted feature vectors,

$$\mathbf{A} = \left[\boldsymbol{v}_{1,1}, \boldsymbol{v}_{1,2}, \ldots, \boldsymbol{v}_{k,n_k}\right] \in R^{m \times n}, \tag{3}$$

where k is the number of classes in the gallery set, n_k is the number of samples for class k, m is the dimension of features, and n is the total number of gallery samples. For robust recognition, we require that $m < n$.

Given a probe 3D palmprint, denote by $\boldsymbol{y} \in R^m$ its feature vector. Then, $\boldsymbol{y}$ can be coded as a linear combination of all the gallery feature vectors, which can be expressed as,

$$\boldsymbol{y} = \mathbf{A}\boldsymbol{x}_0. \tag{4}$$

Since typically $\mathbf{A}$ is a redundant dictionary, the solution to Eq. (4) is not unique. To make the coefficient vector $\boldsymbol{x}_0$ be informative for classification, some kinds of regularization terms need to be added to $\boldsymbol{x}_0$. If an l_1-norm sparsity term is added, the obtained model actually is SRC [35],

$$\boldsymbol{x}_0 = \arg\min_{\boldsymbol{x}} \left\{\|\boldsymbol{y} - \mathbf{A}\boldsymbol{x}\|_2^2 + \lambda_1 \|\boldsymbol{x}\|_1\right\}, \tag{5}$$

where λ_1 is a scalar weight. Eq. (5) does not have a closed-form solution; instead, it can only be solved by iterative optimizations. In the past decade, several efficient methods have been proposed to solve the l_1-minimization problem expressed as Eq. (5), including Homotopy [46], FISTA [47], l_1ls [48], SpaRSA [49], DALM [50], etc.

In [42], Zhang et al. claimed that it is the collaborative representation, i.e., using the training samples from all classes to represent the query sample $\boldsymbol{y}$, but not the l_1-norm sparsity regularization that makes SRC powerful for face recognition. They proposed to

TABLE 2
Algorithm for CR-Based 3D Palmprint Identification

Training phase
Input: A gallery set containing 3D palmprint ROIs.
Output: The dictionary matrix $\mathbf{A}$.
1. For each sample in the gallery set
   Extract from it a feature vector $\boldsymbol{h}$;
   Normalize $\boldsymbol{h}$ to have unit l_2-norm.
2. Concatenate all $\boldsymbol{h}$s as $\mathbf{A}$.

Testing phase
Input: A query 3D palmprint sample and $\mathbf{A}$.
Output: Identity of the query sample.
1. Extract the ROI from the query palmprint.
2. Extract the feature vector $\boldsymbol{y}$ from the ROI.
3. Code $\boldsymbol{y}$ over $\mathbf{A}$ with SRC as,
$$\boldsymbol{x}_0 = \arg\min_{x} \{\|\boldsymbol{y} - \mathbf{A}\boldsymbol{x}\|_2^2 + \lambda_1 \|\boldsymbol{x}\|_1\},$$
or with CRC_RLS as
$$\boldsymbol{x}_0 = \arg\min_{x} \{\|\boldsymbol{y} - \mathbf{A}\boldsymbol{x}\|_2^2 + \lambda_2 \|\boldsymbol{x}\|_2^2\}.$$
4. Compute the residuals $\boldsymbol{r}_i(\boldsymbol{y}) = \|\boldsymbol{y} - \mathbf{A}\delta_i(\boldsymbol{x}_0)\|_2$, where $\delta_i(\boldsymbol{x}_0)$ is a new vector whose only nonzero entries are the entries in $\boldsymbol{x}_0$ that are associated with class i.
5. $\text{Identity}(\boldsymbol{y}) = \arg\min_i \{r_i(\boldsymbol{y})\}$.

replace the l_1-norm sparsity term in SRC framework with an l_2-norm regularization term and the resulting model can be expressed as,

$$\boldsymbol{x}_0 = \arg\min_{\boldsymbol{x}} \{\|\boldsymbol{y} - \mathbf{A}\boldsymbol{x}\|_2^2 + \lambda_2 \|\boldsymbol{x}\|_2^2\}. \tag{6}$$

Such a classification model is named as CRC_RLS (collaborative representation based classification with regularized least square). Fortunately, different from Eq. (5), it can be easily verified that Eq. (6) has a closed-form solution as,

$$\boldsymbol{x}_0 = \left(\mathbf{A}^T\mathbf{A} + \lambda_2\mathbf{I}\right)^{-1}\mathbf{A}^T\boldsymbol{y}. \tag{7}$$

Let $\mathbf{P} = (\mathbf{A}^T\mathbf{A} + \lambda_2\mathbf{I})^{-1}\mathbf{A}^T$. Clearly, $\mathbf{P}$ is independent of $\boldsymbol{y}$ and can be pre-computed totally based on the gallery set.

Since both of SRC and CRC_RLS are based on CR, we refer them as CR-based classification approaches in this paper. The two CR-based classification approaches use the same criterion for classification, i.e., evaluating which class leads to the minimum representation error [35]. With the block-wise statistics based features, the proposed CR-based 3D palmprint identification algorithm is summarized in Table 2. Its general flowchart is illustrated in Fig. 3.

4 Experiments

4.1 Implementation Details

Some details in implementation are presented here. At first, for computing curvatures for range images (see Eq. (1) and Eq. (2)), partial derivatives with various orders need to be estimated. To reliably estimate partial derivatives, we resort to the scheme proposed in [43]. Specifically, the range image is at first smoothed by using a binomial filter and then partial derivatives are computed by convolving with various predefined window masks. The binomial smoothing filter can be written as $\boldsymbol{S} = \boldsymbol{s}\boldsymbol{s}^T$, where the column vector $\boldsymbol{s}$ is given by

$$\boldsymbol{s} = \frac{1}{64}[1\ 6\ 15\ 20\ 15\ 6\ 1]^T. \tag{8}$$

Derivative estimation window masks are defined as $D_x = \boldsymbol{d}_0\boldsymbol{d}_1^T$, $D_y = \boldsymbol{d}_1\boldsymbol{d}_0^T$, $D_{xx} = \boldsymbol{d}_0\boldsymbol{d}_2^T$, $D_{yy} = \boldsymbol{d}_2\boldsymbol{d}_0^T$, and $D_{xy} = \boldsymbol{d}_1\boldsymbol{d}_1^T$, where the column vectors d_0, d_1, and d_2 are given by

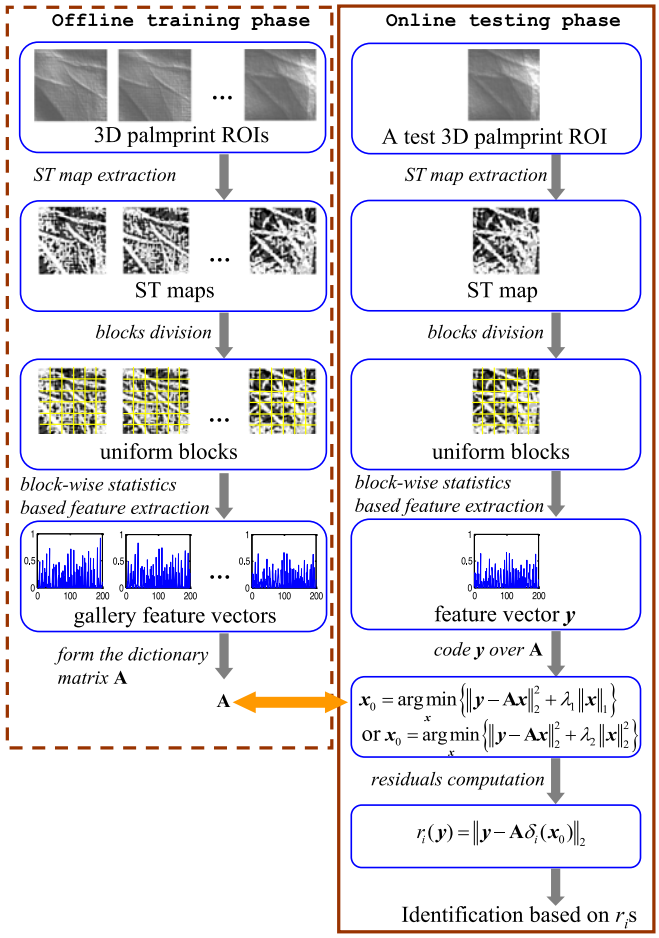

Fig. 3. Illustration for the proposed CR-based framework for 3D palmprint identification.

$$\begin{aligned}
\boldsymbol{d}_0 &= \frac{1}{7}[1\ \ 1\ \ 1\ \ 1\ \ 1\ \ 1\ \ 1]^T \\
\boldsymbol{d}_1 &= \frac{1}{28}[-3\ \ -2\ \ -1\ \ 0\ \ 1\ \ 2\ \ 3]^T \\
\boldsymbol{d}_2 &= \frac{1}{84}[5\ \ 0\ \ -3\ \ -4\ \ -3\ \ 0\ \ 5]^T.
\end{aligned} \tag{9}$$

Then, partial derivative maps of the image $f(x, y)$ are computed as,

$$\begin{aligned}
f_x(x,y) &= \mathbf{D}_x\ {}^*\mathbf{S}^*\ f(x,y), \\
f_y(x,y) &= \mathbf{D}_y\ {}^*\mathbf{S}^*\ f(x,y), \\
f_{xx}(x,y) &= \mathbf{D}_{xx}\ {}^*\mathbf{S}^*\ f(x,y), \\
f_{yy}(x,y) &= \mathbf{D}_{yy}\ {}^*\mathbf{S}^*\ f(x,y), \\
f_{xy}(x,y) &= \mathbf{D}_{xy}\ {}^*\mathbf{S}^*\ f(x,y).
\end{aligned} \tag{10}$$

When computing STs, we need to decide whether the mean curvature H (or the Gaussian curvature K) is 0 or not. However, since both H and K take real values, it is quite rare for them to take the value 0 precisely in practice. Thus, in implementation we adopted the trick mentioned in [20] to decide a symmetric interval $[-\varepsilon_H, \varepsilon_H]$ (or $[-\varepsilon_K, \varepsilon_K]$) covering 0 for quantization. H (K) is deemed as 0 when its value is covered by the interval $[-\varepsilon_H, \varepsilon_H]$ ($[-\varepsilon_K, \varepsilon_K]$). To make the threshold $\varepsilon_H(\varepsilon_K)$ be adaptive to different palms, we normalize H (K) by its standard deviation as suggested by Li et al. [20]. We set $\varepsilon_H = 0.030$ and $\varepsilon_K = 0.015$ in our implementation.

Some other key parameters were set as $\lambda_1 = 0.002$, $\lambda_2 = 0.01$, and $p = 12$.

4.2 Database and Experimental Protocol

In experiments, we used the PolyU 3D palmprint database [21]. This database contains 8,000 samples collected from 400 different palms, belonging to 200 volunteers. Among the volunteers, 136 were male and the other 64 were female. 20 samples from each of these palms were collected in two separated sessions, where 10 samples were captured in each session, respectively. The average time interval between the two sessions was one month.

In the following experiments, we took samples collected at the first session as the gallery set and samples collected at the second session as the probe set. Under such an experimental setting, it is easy to know that for the gallery set, there are 400 classes and for each class there are 10 samples. We use the recognition rate as the performance measure. In addition, the running speed of each competing method was evaluated. Experiments were performed on a standard HP Z620 workstation with a 3.2 GHZ Intel Xeon E5-1650 CPU and an 8 G RAM. The software platform was Matlab R2013b.

4.3 Effectiveness of ST Histograms Based Features

In our CR-based 3D palmprint identification framework, each 3D range image is represented as a feature vector and for feature extraction we propose to use local histograms of STs (LHST) as features. That is, for each range block, we extract from it a histogram of STs and then we concatenate the histograms of all blocks together as the feature vector. In this section, to demonstrate the effectiveness of the proposed feature extraction scheme LHST, we compared its performance with several other kinds of features existing in the literature. In order to evaluate the performance of different features, we need to fix the classification approach. In this experiment, with respect to the classification framework, we used CRC_RLS.

The local histogram of STs can be viewed as a kind of local statistics based features. Actually, in the literature there are also other local statistics based features. For example, local binary pattern has been testified to be a powerful descriptor for many image classification tasks [15], [51]. When using LBP, actually we regard the range image data as standard image data. In this experiment, when extracting LBP-based features, for each 3D palmprint ROI, we divided it into uniform blocks, extracted local histogram of LBP from each block, and then concatenated all the histograms to form the final feature vector. An LBP operator can be represented as $LBP^{riu2}_{P,R}$, where "riu2" means the use of *r*otation *i*nvariant *u*niform patterns that have transitions at most 2, R is the sampling radius and P is the number of sampling points. We tested three LBP operators $LBP^{riu2}_{8,1}$, $LBP^{riu2}_{16,3}$, and $LBP^{riu2}_{24,5}$, and also their combinations denoted by LBP_m.

Local orientation coding based methods have been testified to be quite successful in the fields of 2D biometrics. For example, CompCode [10], which encodes the local orientation using a set of Gabor filters, is a quite powerful method for matching 2D palmprints. In this experiment, we tested its performance for 3D palmprint classification. Specifically, for each block, we extract from it a histogram of CompCode and then form the feature vector by concatenating all the local histograms.

In addition, we also tested the performance of vectorized MCI, GCI and ST maps [20] as feature vectors. Details for computing MCI, GCI and ST maps can be found in [20].

The evaluation results are summarized in Table 3. From Table 3, it can be clearly observed that as a feature extraction scheme, the proposed method LHST based on block-wise ST histograms performs much better than all the other methods evaluated. It indicates that such a feature extraction scheme have a stronger capability in characterizing local shape structures of 3D range data. Consequently, in the following Section 4.4, for the proposed CR-based 3D palmprint identification approaches, we use the local histograms of STs as features.

TABLE 3
Recognition Rates by Using Different Features

	recognition rate
$LBP^{riu2}_{8,1}$	0.8080
$LBP^{riu2}_{16,3}$	0.8720
$LBP^{riu2}_{24,5}$	0.9023
LBP_m	0.9175
CompCode	0.9440
MCI	0.9355
GCI	0.6710
ST	0.9215
LHST	0.9915

4.4 Performance Evaluation and Discussions

In this experiment, the performance of competing methods was evaluated. In our proposed CR-based 3D palmprint identification framework, we use local histograms of surface types as features. With respect to the regularization term, l_1-norm sparsity term or the l_2-norm term can be used. If the l_2-norm term is used, we refer this method as $\mathrm{CR\_L_2}$. If the l_1-norm sparsity term is used, we tried different methods to solve the l_1-minimization problem, including Homotopy [46], FISTA [47], l_1_ls [48], SpaRSA [49], DALM [50]. And accordingly, we refer these methods as $\mathrm{CR_L_1}$_Homotopy, $\mathrm{CR_L_1}$_FISTA, $\mathrm{CR\_L_1}l_1\_ls$, $\mathrm{CR_L_1}$_SpaRSA, and $\mathrm{CR_L_1}$_DALM, respectively. As suggested by one reviewer, in order to show the superiority of CR-based schemes for classification, we also tested the approach which matches LHST feature vectors by using the Chi-square distance, which is defined as,

$$\chi^2(\boldsymbol{f},\boldsymbol{g}) = \sum_{n=1}^{N} (\boldsymbol{f}_n - \boldsymbol{g}_n)^2/(\boldsymbol{f}_n + \boldsymbol{g}_n), \tag{11}$$

where $\boldsymbol{f}$ and $\boldsymbol{g}$ are two histograms with N bins, $\boldsymbol{f}_n(\boldsymbol{g}_n)$ is the value of $\boldsymbol{f}$ ($\boldsymbol{g}$) at the nth bin. Chi-square distance is a widely used metric for matching two histogram-like feature vectors [51]. We refer this method as LHST_ChiSquare.

Several other state-of-the-art methods for 3D palmprint matching were also evaluated. They include the mean curvature image-based method [20], the Gaussian curvature image-based method [20], the surface types-based method [20], and the local correlation (LC)-based method [24].

The evaluation results are summarized in Table 4. In Table 4, we list the recognition rate achieved by each method. In addition, we also list the time cost consumed for one identification operation by each method. Given a test sample, the time cost for one identification operation includes the time consumed by the feature extraction and the time consumed by matching the test feature with the gallery feature set.

Based on the evaluation results listed in Table 4, we could have the following findings. At first, with respect to the classification accuracy, the proposed CR-based approaches perform much better than the other state-of-the-art methods. Particularly, MCI [20], GCI [20], and LC [24] cannot obtain comparable performance with the other methods. Moreover, LHST_ChiSquare performs poorer than the CR-based ones though they utilize the same set of features. It indicates that for classification CR-based schemes perform better than the Chi-square distance based matching.

Second, all the CR-based methods, no matter the l_1-norm regularization term is used or the l_2-norm regularization term is used, can lead to quite similar results. Such a result again validates Zhang et al.'s claim that it is the collaborative representation, not the l_1-norm based sparsity regularization term, which makes SRC quite powerful for classification [42]. However, a CR model with an l_2-norm regularization (Eq. (6)) can be greatly easier and much more efficiently solved than a CR model with an l_1-norm

TABLE 4
Experimental Results by Using Various Methods

	recognition rate	time cost for 1 identification (ms)
CR_l_1_Homotopy	0.9925	321.70
CR_l_1_FISTA	0.9942	10,905.26
CR_l_1_l_1_ls	0.9935	14,054.62
CR_l_1_SpaRSA	0.9882	2,131.42
CR_l_1_DALM	0.9948	547.03
LHST_ChiSquare	0.9593	55.78
MCI [20]	0.9188	9,403.33
GCI [20]	0.9187	9,403.30
ST [20]	0.9878	63,275.86
LC [24]	0.9173	70,992.13
CR_L_2	**0.9915**	**22.78**

regularization (Eq. (5)). Thus, the method CR_L_2 is highly preferred, at least for the task of 3D palmprint identification.

Third, in terms of the running speed, CR_L_2 runs much faster than all the other methods evaluated. Under our experimental settings, it costs CR_L_2 only 22.78 ms to complete one identification operation against a gallery set comprising 4,000 samples from 400 classes. The low speeds of MCI, GCI, and ST [20] should be attributed to the multiple translation-based matching strategy they adopted. That is, in order to account for the possible translation between the probe ROI t and the gallery ROI r, multiple matches are performed by translating one set of feature maps in horizontal and vertical directions and the minimum of the resulting matching distances is considered to be the final matching distance between t and r. For LC [24], it needs to compute a local correlation coefficient for every point, which makes it rather slow. For the CR-based methods using l_1-norm sparsity regularizations, their running speeds vary a lot. This should be attributed to the different l_1-minimization techniques they adopt. From our evaluations it can be seen that Homotopy and DALM are more efficient than FISTA, l_1_ls, and SpaRSA.

Based on the above discussions, we recommend using the CR_L_2 method with local histograms of STs as features for 3D palmprint identification since such an approach can achieve a distinguished high recognition accuracy while maintaining an extremely low computational complexity. It is quite suitable for large-scale identification applications.

5 Conclusions

In this paper, we propose to use the collaborative representation based classification framework for 3D palmprint identification. Under the CR framework, l_1-norm or l_2-norm regularizations are usually required for the classification task. Our experimental results indicate that l_2-norm based regularization is much more efficient than l_1-norm based regularization while they can achieve nearly the identical recognition accuracy. Another contribution is that we proposed a local histograms of surface types based feature extraction method, which is quite effective and robust to mere misalignments. The recognition rate of our method on PolyU benchmark data set is 99.15 percent. With our method (implemented in Matlab), the time cost for one identification operation against a gallery set comprising 4,000 samples from 400 classes is merely 22.78 ms on a standard workstation.

Acknowledgments

This work was supported in part by the Natural Science Foundation of China under grant no. 61201394, in part by the National Basic Research Program of China under grant no. 2013CB967101, in part by the Shanghai Pujiang Program under grant nos. 13PJ1408700, 13PJ1433200, and 14PJ1408100, and in part by the Jiangsu Key Laboratory of Image and Video Understanding for Social Safety (Nanjing University of Science and Technology) under grant no. 30920140122007.

References

[1] A. K. Jain and J. Feng, "Latent palmprint matching," *IEEE Trans. Pattern Anal. Mach. Intell.*, vol. 31, no. 6, pp. 1032–1047, Jun. 2009.
[2] D. R. Ashbaugh, *Quantitative-Qualitative Friction Ridge Analysis: Introduction to Basic Ridgeology*. Boca Raton, FL, USA: CRC Press, 1999.
[3] H. Cummins and M. Midlo, *Finger Prints, Palms and Soles: An Introduction to Dermatoglyphics*. New York, NY, USA: Dover, 1961.
[4] D. Zhang, W. K. Kong, J. You, and M. Wong, "Online palmprint identification," *IEEE Trans. Pattern Anal. Mach. Intell.*, vol. 25, no. 9, pp. 1041–1050, Sep. 2003.
[5] PolyU Palmprint Database (Jun., 2014). [Online]. Available: www.comp.polyu.edu.hk/∼biometrics/
[6] W. Jia, D. Huang, and D. Zhang, "Palmprint verification based on principal lines," *Pattern Recognit.*, vol. 41, no. 4, pp. 1316–1328, Apr. 2008.
[7] L. Shang, D. Huang, J. Du, and C. Zheng, "Palmlprint recognition using FastICA algorithm and radial basis probabilistic neural network," *Neurocomputing*, vol. 69, no. 13, pp. 1782–1786, Aug. 2006.
[8] X. Wu, D. Zhang, and K. Wang, "Fisherpalms based palmprint recognition," *Pattern Recognit. Lett.*, vol. 24, no. 15, pp. 2829–2838, Nov. 2003.
[9] L. Zhang and D. Zhang, "Characterization of palmprints by wavelet signatures via directional context modeling," *IEEE Trans. Syst., Man Cybern., Part B*, vol. 34, no. 3, pp. 1335–1347, Jun. 2004.
[10] A. Kong and D. Zhang, "Competitive coding scheme for palmprint verification," in *Proc. Int. Conf. Pattern Recognit.*, 2004, pp. 520–523.
[11] Z. Sun, T. Tan, Y. Wang, and S. Z. Li, "Ordinal palmprint representation for personal identification," in *Proc. IEEE Int. Conf. Comput. Vis. Pattern Recognit.*, 2005, pp. 279–284.
[12] W. Zuo, Z. Lin, Z. Guo, and D. Zhang, "The multiscale competitive code via sparse representation for palmprint verification," in *Proc. IEEE Int. Conf. Comput. Vis. Pattern Recognit.*, 2010, pp. 2265–2272.
[13] L. Zhang and H. Li, "Encoding local image patterns using Riesz transforms: With applications to palmprint and finger-knuckle-print recognition," *Image Vis. Comput.*, vol. 30, no. 12, pp. 1043–1051, Dec. 2012.
[14] G. K. O. Michael, T. Connie, and A. B. J. Teoh, "Touch-less palm print biometrics: Novel design and implementation," *Image Vis. Comput.*, vol. 26, no. 12, pp. 1551–1560, Dec. 2008.
[15] T. Ojala, M. Pietikainen, and T. Maenpaa, "Multiresolution gray-scale and rotation invariant texture classification with local binary patterns," *IEEE Trans. Pattern Anal. Mach. Intell.*, vol. 24, no. 7, pp. 971–987, Jul. 2002.
[16] Data format for the interchange of fingerprint facial, & other biometric information. (2012). [Online]. Available: ANSI/NIST-ITL, 1-2007, http://www. nist.gov/customcf/get_pdf.cfm?pub_id = 51174
[17] J. Dai and J. Zhou, "Multifeature-based high-resolution palmprint recognition," *IEEE Trans. Pattern Anal. Mach. Intell.*, vol. 33, no. 5, pp. 945–957, May 2011.
[18] J. Dai, J. Feng, and J. Zhou, "Robust and efficient ridge-based palmprint matching," *IEEE Trans. Pattern Anal. Mach. Intell.*, vol. 34, no. 8, pp. 1618–1632, Aug. 2012.
[19] W. Li, D. Zhang, G. Lu, and N. Luo, "A novel 3-D palmprint acquisition system," *IEEE Trans. Syst., Man Cybernetics, Part A*, vol. 42, no. 2, pp. 443–452, Mar. 2012.
[20] D. Zhang, G. Lu, W. Li, L. Zhang, and N. Luo, "Palmprint recognition using 3-D information," *IEEE Trans. Syst., Man Cybernetics, Part C*, vol. 39, no. 5, pp. 505–519, Sep. 2009.
[21] (Jun., 2014). [Online]. Available: PolyU 2D and 3D Palmprint Database, www.comp.polyu.edu. hk/∼biometrics/
[22] W. Li, L. Zhang, D. Zhang, G. Lu, and J. Yan, "Efficient joint 2D and 3D palmprint matching with alignment refinement," in *Proc. IEEE Int. Conf. Comput. Vis. Pattern Recognit.*, 2010, pp. 795–801.
[23] W. Li, D. Zhang, L. Zhang, G. Lu, and J. Yan, "3-D palmprint recognition with joint line and orientation features," *IEEE Trans. Syst., Man Cybernetics, Part C*, vol. 41, no. 2, pp. 274–279, Mar. 2011.
[24] D. Zhang, V. Kanhangad, N. Luo, and A. Kumar, "Robust palmprint verification using 2D and 3D features," *Pattern Recognit.*, vol. 43, no. 1, pp. 358–368, Jan. 2010.
[25] B. Yang, X. Wang, J. Yao, X. Yang, and W. Zhu, "Efficient local representations for three-dimensional palmprint recognition," *J. Electron. Imaging*, vol. 22, no. 4, p. 043040, Oct. 2013.
[26] M. Liu and L. Li, "Cross-correlation based binary image registration for 3D palmprint recognition," in *Proc. Int. Conf. Signal Process.*, 2012, pp. 1597–1600.
[27] J. Cui, "2D and 3D palmprint fusion and recognition using PCA plus TPTSR method," *Neural Comput. Appli.*, vol. 24, no. 3, pp. 497–502, Mar. 2014.
[28] J. G. Daugman, "High confidence visual recognition of persons by a test of statistical independence," *IEEE Trans. Pattern Anal. Mach. Intell.*, vol. 15, no. 11, pp. 1148–1161, Nov. 1993.
[29] P. J. Besl and N. D. Mckay, "A method for registration of 3-D shapes," *IEEE Trans. Pattern Anal. Mach. Intell.*, vol. 14, no. 2, pp. 239–256, Feb. 1992.

[30] Y. Xu Y, D. Zhang, J. Yang, J. Yang, "A two-phase test sample sparse representation method for use with face recognition," *IEEE Trans. Circuits Syst. Video Technol.*, vol. 21, no. 9, pp. 1255–1262, Sep. 2011.
[31] H. Drira, B. B. Amor, A. Srivastava, M. Daoudi, and R. Slama, "3D face recognition under expressions, occlusions, and pose variations," *IEEE Trans. Pattern Anal. Mach. Intell.*, vol. 35, no. 9, pp. 2270–2283, Sep. 2013.
[32] L. Zhang, Z. Ding, H. Li, Y. Shen, and J. Lu "3D face recognition based on multiple keypoint descriptors and sparse representation," *PLoS One*, vol. 9, no. 6, p. e100120, Jun. 2014.
[33] S. M. Islam, R. Davies, M. Bennamoun, and A. S. Mian, "Efficient detection and recognition of 3D ears," *Int. J. Comput. Vis.*, vol. 95, no. 1, pp. 52–73, Oct. 2011.
[34] L. Zhang, Z. Ding, H. Li, and Y. Shen, "3D ear identification based on sparse representation," *PLoS One*, vol. 9, no. 4, p. e95506, Apr. 2014.
[35] J. Wright, A. Y. Yang, A. Ganesh, S. S. Sastry, and Y. Ma, "Robust face recognition via sparse representation," *IEEE Trans. Pattern Anal. Mach. Intell.*, vol. 31, no. 2, pp. 210–227, Feb. 2009.
[36] A. Wagner, J. Wright, A. Ganesh, Z. Zhou, H. Mobahi, and Y. Ma, "Towards a practical face recognition system: Robust alignment and illumination by sparse representation," *IEEE Trans. Pattern Anal. Mach. Intell.*, vol. 34, no. 2, pp. 372–386, Feb. 2012.
[37] Y. Peng, A. Ganesh, J. Wright, W. Xu, and Y. Ma, "RASL: Robust alignment by sparse and low-rank decomposition for linearly correlated images," *IEEE Trans. Pattern Anal. Mach. Intell.*, vol. 34, no. 11, pp. 2233–2246, Nov. 2012.
[38] M. Yang, L. Zhang, X. Feng, and D. Zhang, "Fisher discrimination dictionary learning for sparse representation," in *Proc. Int. Conf. Comput. Vis.*, 2011, pp. 543–550.
[39] J. K. Pillai, V. M. Patel, R. Chellappa, and N. K. Ratha, "Secure and robust iris recognition using random projections and sparse representation," *IEEE Trans. Pattern Anal. Mach. Intell.*, vol. 33, no. 9, pp. 1877–1893, Sep. 2011.
[40] D. Donoho, "For most large underdetermined systems of linear equations the minimal l_1-norm solution is also the sparsest solution," *Commun. Pure Applied Math.*, vol. 59, no. 6, pp. 797–829, 2006.
[41] R. Rigamonti, M. A. Brown, and V. Lepetit, "Are sparse representations really relevant for image classification?" in *Proc. IEEE Int. Conf. Comput. Vis. Pattern Recognit.*, 2011, pp. 1545–1552.
[42] L. Zhang, M. Yang, and X. Feng, "Sparse representation or collaborative representation: Which helps face recognition?" in *Proc. Int. Conf. Comput. Vis.*, 2011, pp. 471–478.
[43] P. J. Besl and R. C. Jain, "Segmentation through variable-order surface fitting," *IEEE Trans. Pattern Anal. Mach. Intell.*, vol. 10, no. 2, pp. 167–192, Mar. 1988.
[44] M. P. Do Carmo, *Differential Geometry of Curves and Surfaces*. Englewood Cliffs, NJ, USA: Prentice-Hall, 1976.
[45] J. Flusser, B. Zitova, and T. Suk, *Moments and Moment Invariants in Pattern Recognition*. Hoboken, NJ, USA: Wiley, 2009.
[46] D. Malioutov, M. Cetin, and A. Willsky, "Homotopy continuation for sparse signal representation" in *Proc. IEEE Int. Conf. Acoustics, Speech, Signal Process.*, 2005, pp. 733–736.
[47] A. Beck and M. Teboulle, "A fast iterative shrinkage-thresholding algorithm for linear inverse problems," *SIAM J. Imaging Sci.*, vol. 2, no. 1, pp. 183–202, 2009.
[48] S. J. Kim, K. Koh, M. Lustig, S. Boyd, and D. Gorinevsky, "An interior-point method for large-scale l_1-regularized least squares," *IEEE J. Sel. Topics Signal Process.*, vol. 1, no. 4, pp. 606–617, Dec. 2007.
[49] S. J. Wright, R.D Nowak, M. A. T. Figueiredo, "Sparse reconstruction by separable approximation," *IEEE Trans. Signal Process.*, vol. 57, no. 7, pp. 2479–2493, Jul. 2009.
[50] J. Yang and Y. Zhang, "Alternating direction algorithms for l_1-problems in compressive sensing," *SIAM J. Sci. Comput.*, vol. 33, no. 1, pp. 250–278, 2011.
[51] L. Zhang, Z. Zhou, and H. Li, "Binary Gabor pattern: An efficient and robust descriptor for texture classification," in *Proc. IEEE Int. Conf. Image Process.*, 2012, pp. 81–84.